Experiments on Arrays of Globally Coupled Periodic Electrochemical Oscillators

István Z. Kiss,† Wen Wang, and J. L. Hudson*

Department of Chemical Engineering, Thornton Hall, University of Virginia, Charlottesville, Virginia 22903-2442

Received: July 20, 1999; In Final Form: October 11, 1999

Experiments on periodically oscillating arrays consisting of from one to 64 nickel electrodes in sulfuric acid are carried out. Harmonic and relaxation oscillations that occur respectively in two regions of parameter space are considered. External resistors in parallel and series are added to vary the extent of global coupling among the oscillators. The array is heterogeneous due to small variations in the properties of the electrodes, and there is also a small amount of noise. With no added global coupling there is a narrow distribution in frequency of the oscillators. As global coupling is added to the arrays of harmonic oscillators the distribution of frequencies become narrower until synchronization is attained; further increase brings the phases together. There is no qualitative change in the dynamics of an individual element. Coupling of the relaxation oscillators leads to more complicated behavior. As the global coupling strength is increased from zero there is a tendency for the system to synchronize, but this synchronized state then breaks up with increasing coupling. Irregular behavior including transient clusters then occurs. At stronger coupling the clusters become stable; these stable clusters can consist of individual currents that are either irregular or periodic with higher period. Multistability occurs in this region, i.e, many cluster configurations are possible. At higher coupling strengths antiphase oscillations occur where the clusters are made up of equal or approximately equal number of oscillators. Strong coupling synchronizes the oscillators. Simulations based on coupled electrochemical oscillators reproduced many of the dynamical features.

Introduction

Electrochemical systems have been studied extensively using the tools of nonlinear dynamics. A plethora of types of dynamical behavior have been observed and discussed in some recent reviews.[1−6] The rate of reaction often varies with both time and position, and the range and strength of the coupling between sites influence the types of patterns that can be observed.[7−18]

In electrochemical systems a nonlocal coupling among reactive sites arises through the electric field; potential changes at some location are transmitted rapidly to other locations. This coupling is long range but is not global because its effect dies out with increasing distance.

In addition, a global coupling can be imposed on electrochemical systems simply through the addition of an external resistance.[19,20] When an overall potential is imposed on a system (potentiostatic operation), potential drops through the resistance influence the potential of the working electrode (reacting surface); thus this coupling is global. Galvanostatic operation (constant imposed current) has an intrinsic constraint since the condition of constant total current implies that changes at any location are felt globally.

The influence of global coupling on spatiotemporal pattern formation is also important in other types of chemical reactions such as gas−solid systems. Mixing in the gas phase produces a global coupling because a consumption of reactants or production of products at one location causes changes in conditions at all locations of the system.[21−23] Such a coupling can have a strong role in altering pattern formation[24,25] and in stabilizing patterns in nonuniform systems.[26] Global coupling through an external control or an integral constraint has also been investigated.[27,28]

One method of determining the spatiotemporal structure in the electrochemical systems is with the use of electrode arrays.[29−31] The arrays consist of a number of small disks that are made from the end of wires embedded in an insulator. One advantage of the arrays is that the individual currents can be measured and thus the rate of reaction as a function of position and time can be found. Since the coupling is largely long range and through the electrolyte, an array can exhibit overall behavior that is similar to that of a single electrode of the same total area. For example, excellent agreement has been found in the iron−sulfuric acid system between activation and passivation waves on arrays and on a single larger disk.[29] Furthermore, similar behavior of arrays and single electrode systems has been found in the chaotic region where faster oscillations occur.[30]

In the present work we investigate the anodic electrodissolution of Ni in sulfuric acid. The temporal and spatiotemporal behavior of the system was studied by Lev et al.[32−35] and bistability as well as periodic, chaotic, and quasiperiodic oscillations were observed under galvanostatic and potentiostatic conditions using an external resistor. Spatiotemporal patterns including travelling and standing waves were observed.

We investigate periodic oscillators that are coupled largely through global coupling. In electrochemical systems the coupling strengths can be varied by changing the concentration of the electrolyte and by variations of the cell geometry. However, in making either of these changes the potential drop across the electrical double layer would also be changed. In this work we describe a method of altering the strength of global coupling while holding all other parameters constant. This is done through the use of external resistors; the total external resistance is held

† Permanent address: Institute of Physical Chemistry, Kossuth Lajos University, Debrecen H-4010, Hungary.

10.1021/jp992471h CCC: $18.00
Published on Web 12/07/1999

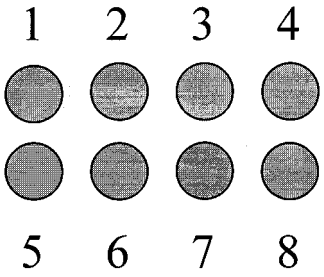

Figure 1. Schematic of array.

constant while the fraction dedicated to individual currents, as opposed to the total current, can be varied. Since the electrolyte concentration is high, the external resistance is larger than that of the electrolyte and the added global coupling dominates over the nonglobal coupling inherent in the system.

As in any experimental system the array is slightly heterogeneous due to small variations in the properties of the electrodes, and there is also a small amount of noise. With no added global coupling there is a slight variance in both frequency and amplitude of the oscillators. We investigate the effect of coupling both under conditions in which the coupling leads to simple synchronization of the oscillators without inherent qualitative changes in the dynamics and under conditions in which the coupling leads to qualitative changes and to the production of antiphase oscillations, clusters, irregular oscillations, etc.

Experimental Section

The configuration of the array consisting of eight electrodes is shown in Figure 1. Each electrode is made from pure Ni wires (Aldrich Chemical Co., 99.99+%). For the arrays of up to eight electrodes, the diameters of the wires were 2 mm and the distance between them was about 1 mm. The electrodes are embedded in epoxy, and reaction takes place only at the ends. The electrode array is polished with a series of 200−800 grit silicon carbide sandpaper before each experiment. For the experiments one, two (1,5 2,6 3,7 4,8), three (1,2,3 or 5,6,7), four (1,2,5,6 or 3,4,6,7), eight, and sixty-four electrodes were used to study the effect of the increasing number of electrodes. The 64-electrode array (8 × 8 geometry) was made using electrodes of diameter 1 mm.

The electrode array was used as a working electrode in a standard three-electrode electrochemical cell shown in Figure 2. For convenience, only a three-electrode array is shown. The potential of all of the electrodes in the array is held constant using a potentiostat (EG&G Princeton Applied Research, model 273) vs $Hg/Hg_2SO_4/K_2SO_4$ reference electrode. The electrodes are connected to the potentiostat through individual resistors, connected to each of the electrodes, and one collective resistor. To adjust the proper resistors Elektroflex EF-499 (Szeged, Hungary) computer-controlled resistors were installed. Zero resistance ammeters (ZRAs) were used to measure the currents

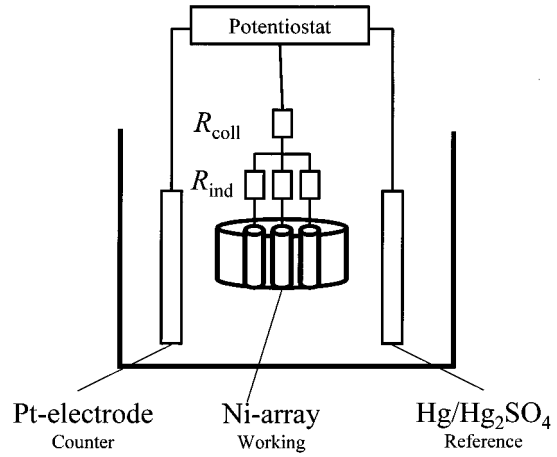

Figure 2. Apparatus.

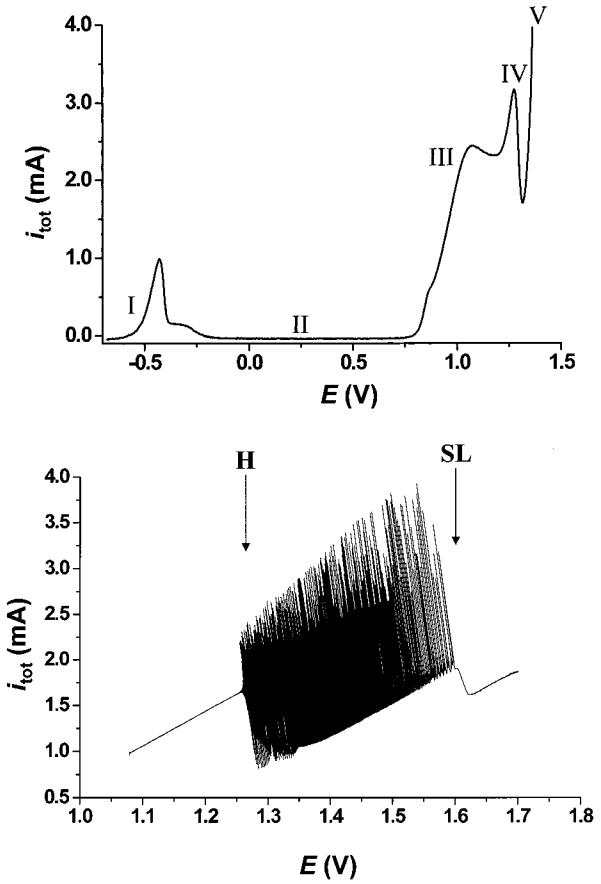

Figure 3. Anodic polarization curves of the Ni−sulfuric acid system. (a) IR-compensated scan (compensated resistance: 2.5 Ω) with a scan rate of 10 mV/s. (b) Scan for single electrode using R_{eq} = 200 Ω external resistance. Scan rate of the potential was 1 mV/s. *E* is the true potential of the working electrode obtained by subtracting the IR drop through external (200 Ω) and solution resistance (3 Ω) from the applied potential V.

of the electrodes independently. The ZRA circuitry was inserted between the individual and collective resistors. The potential converted by the ZRA box was digitized using a transputer, which was connected to a Pentium PC. Testpoint software was used to visualize and save the data. The data acquisition was done at 200 Hz for all data shown. The independent total current was also measured from the potentiostat. The addition of individual currents gave the measured total current within experimental error (0.015 mA).

Experiments were carried out in 4.5 M H_2SO_4 solution

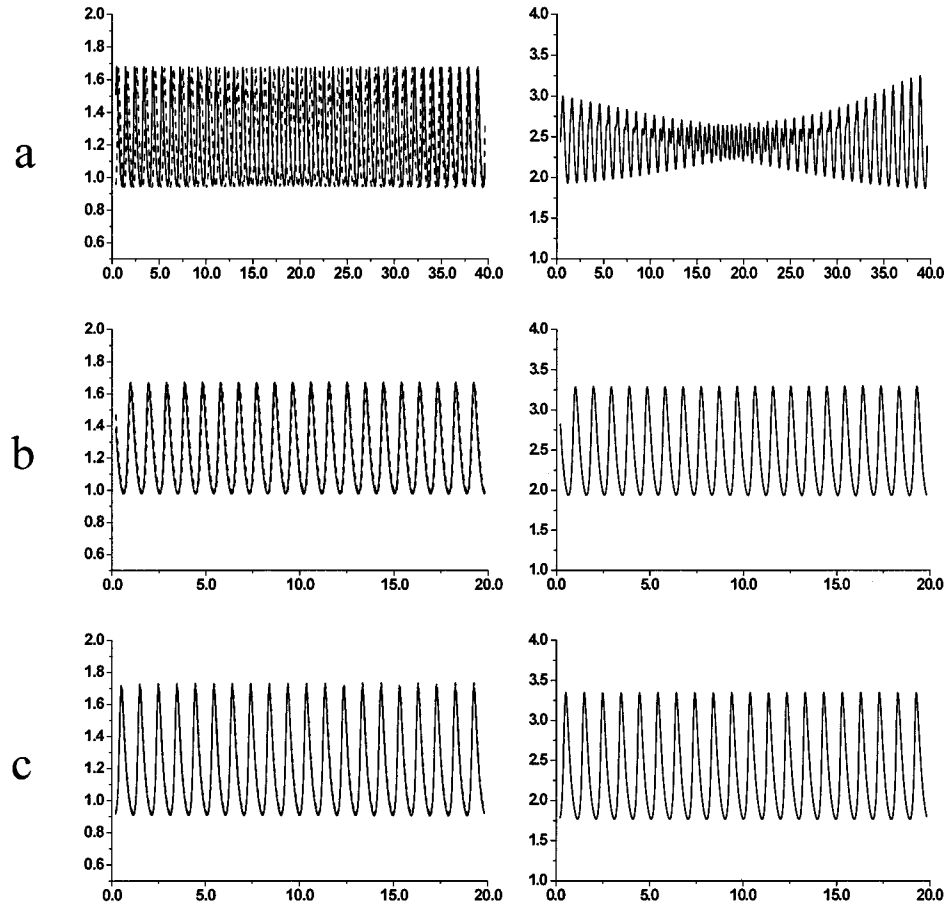

Figure 4. Two electrodes near Hopf bifurcation ($V = 1.257$ V, $R_{eq} = 260\ \Omega$). Individual (left column) and total (right column) currents (mA) vs time (s). (a) $\epsilon = 0.0$; (b) $\epsilon = 0.03$; (c) $\epsilon = 1.0$.

directly diluted from 5M sulfuric acid. N_2 was bubbled through the solution for half an hour prior to each experiment. The counter electrode is Pt sheet. To increase the reproducibility of the experiments the cell was thermostated at 11 °C.

Dynamics of a Single Electrode: Polarization Scans. An IR-compensated anodic polarization scan for a single electrode is shown in Figure 3a. Five different regions can be identified[3] as shown on the figure. Active dissolution (I) and primary passivity (II, the formation of an oxide film) occur at lower potentials. In the transpassive region secondary dissolution of the metal occurs (III) which develops into the regime of secondary passivity (IV) and O_2 evolution (V).

The nickel−sulfuric acid system does not oscillate unless a resistor is connected to the cell under the conditions of these experiments.

In Figure 3b a (not-IR-compensated) polarization scan with an added external resistance is shown in the potential region of transpassive dissolution. At low values of the applied potential no oscillations are seen. With increasing potential a Hopf bifurcation occurs and harmonic oscillations develop. There is then a wide parameter region in which oscillations occur. The oscillations cease in the high potential region through a saddle-loop bifurcation. Below the saddle-loop bifurcation there is a region of relaxation oscillations. Discussions of the dynamics of the nickel−sulfuric acid system can be found in the reviews of Koper[3] and Krischer.[5] As pointed out by these authors, the system belongs to the class of HNDR (hidden negative differential resistance) oscillators.

In this work the behavior will be studied under constant potential conditions in two regions. The first is for low values of the potential near the Hopf bifurcation in which relatively small amplitude, harmonic oscillations occur. The amplitude increases and the frequency decreases as the applied potential is raised; this has already been shown in previous studies.[4] The second is at high values of the potential near the saddle-loop bifurcation; in this region relaxation-type oscillations are observed.

Coupling Parameter. If we have more than one electrode then there are two ways of connecting the external resistors to the cell (see Figure 2). One way is individually (R_{ind}) and the other is collectively (R_{coll}). A total resistance (R_{tot}) can be defined as

$$R_{tot} = R_{coll} + \frac{R_{ind}}{n} \tag{1}$$

where n is the number of electrodes.

It is sometimes useful to refer to an equivalent resistance (R_{eq})

$$R_{eq} = nR_{tot} \tag{2}$$

which gives the equivalent individual resistor that should be inserted into the circuit to observe the same potential drop on the electrode. The use of R_{eq} is helpful in comparing the results of the experiments on different numbers of electrodes in the array.

The collective resistor couples the electrodes globally: the current on one electrode affects the dynamics of the other electrodes since current through any given electrode influences the potential drop on all electrodes equally. The collective resistance fraction (ϵ) expresses the fraction of total collective

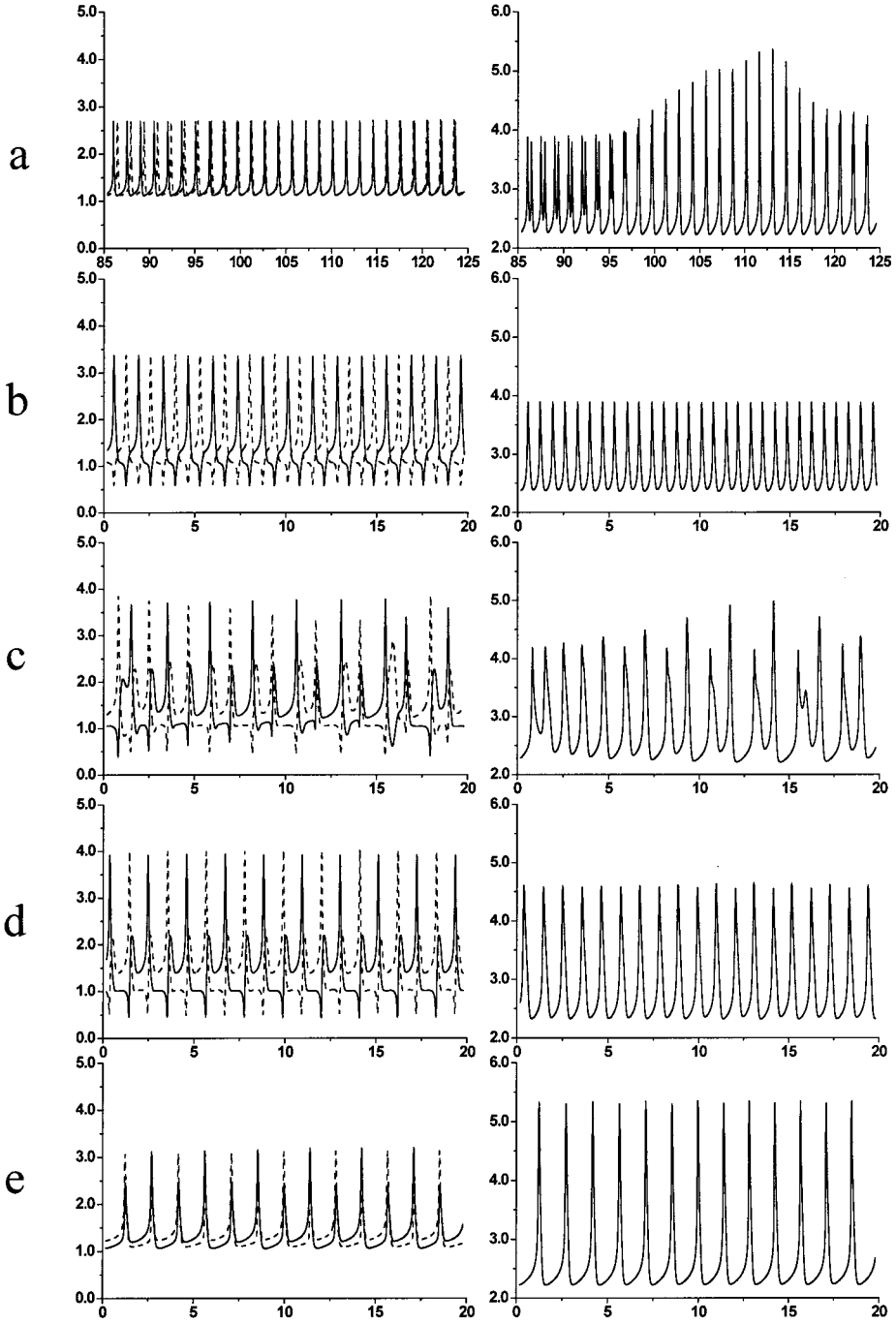

Figure 5. Two electrodes near saddle-loop bifurcation ($V = 1.480$ V, $R_{eq} = 260\ \Omega$). Individual (left column) and total (right column) currents (mA) vs time (s). (a) $\epsilon = 0.0$; (b) $\epsilon = 0.6$; (c) $\epsilon = 0.8$; (d) $\epsilon = 0.9$; (e) $\epsilon = 1.0$.

resistance

$$\epsilon = \frac{R_{coll}}{R_{tot}} \tag{3}$$

This value of ϵ provides a convenient way of expressing the global coupling in the system. If $\epsilon = 0$ then the external resistance furnishes no additional global coupling. If $\epsilon = 1$ then only the maximal external global coupling is achieved. Note that there is intrinsically in the system an additional long-range coupling because of potential drops in the electrolyte and in the external circuitry. In our case this is low ($2-3\ \Omega$). Thus we have an (added) global coupling parameter that takes on values from zero to one as the global coupling increases.

Results

Harmonic Oscillations. Consider first the coupling of the small amplitude harmonic oscillations that occur in the vicinity of the Hopf bifurcation.

Although great care is taken to produce an array of identical electrodes, certain differences are unavoidable and also some amount of noise is present in the system. We are thus dealing with a heterogeneous system of slightly different oscillators. The degree of heterogeneity and noise can most easily be seen in the largest system that was considered, viz., the array of 64 electrodes. For no added global coupling ($\epsilon = 0.0$) the 64 almost independently oscillating electrodes had a mean frequency of 1.44 Hz with a standard deviation of about 0.02 Hz. (We do not have enough resolution to determine the exact distribution

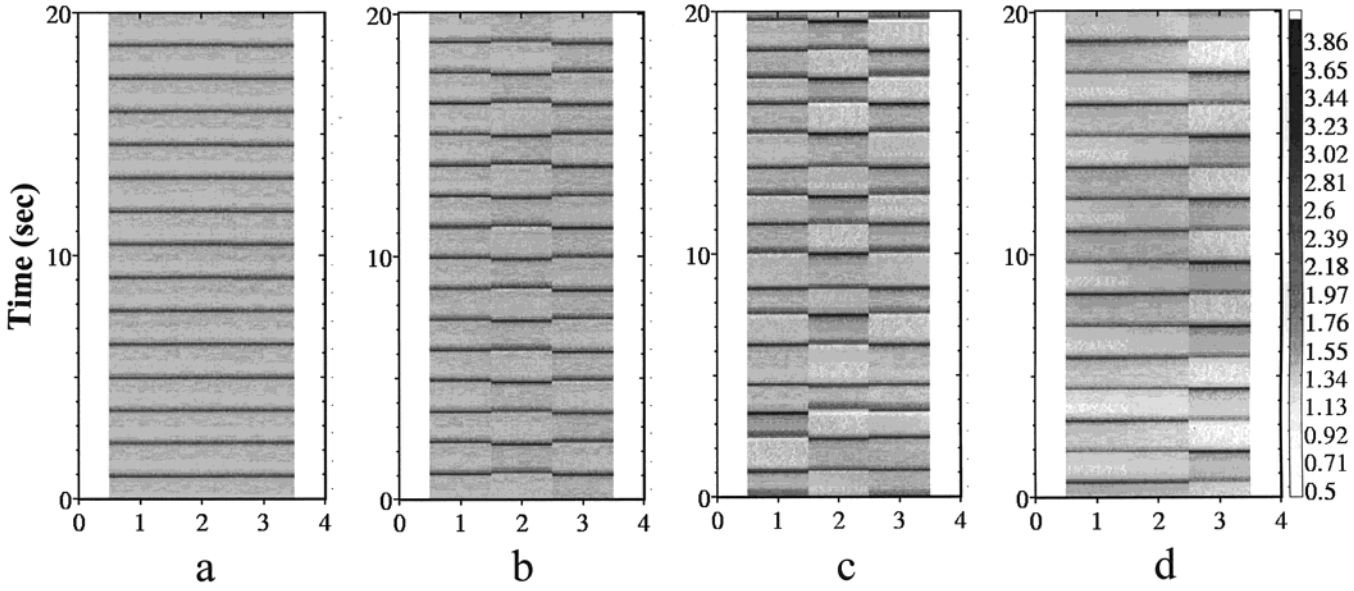

Figure 6. Three electrodes near saddle-loop bifurcation ($V = 1.505$ V, $R_{eq} = 300\ \Omega$). Gray scale plots of individual currents; dark corresponds to high current. (a) $\epsilon = 0.2$; (b) $\epsilon = 0.5$; (c) $\epsilon = 0.8$; (d) $\epsilon = 1.0$.

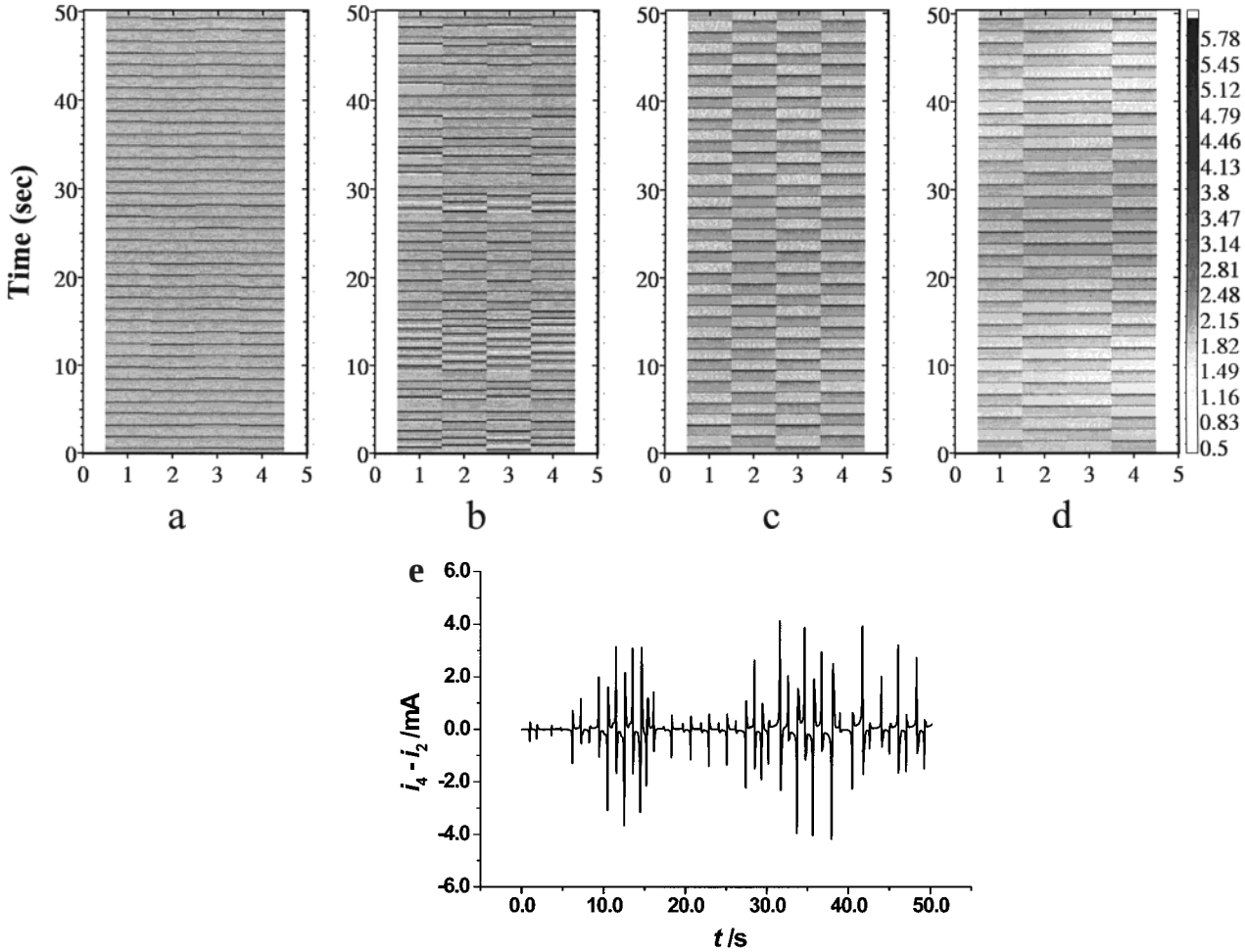

Figure 7. Four electrodes near saddle-loop bifurcation ($V = 1.520$ V, $R_{eq} = 180\ \Omega$). Gray scale plots; dark corresponds to high currents. (a) $\epsilon = 0.22$; (b) $\epsilon = 0.67$; (c) $\epsilon = 1.0$; (d) $\epsilon = 1.0$ (another experiment); (e) Difference between currents of electrodes number 4 and 2 at $\epsilon = 0.67$.

of the frequencies; it is not quite symmetrical about the mean, but rather somewhat skewed toward the higher frequencies.) As the global coupling is increased, the frequency distribution becomes less broad and at $\epsilon = 0.11$ the behavior becomes synchronized; all oscillators have the same frequency. Even at synchronization, however, they are not yet in phase. At a global coupling of $\epsilon = 0.17$ the phases are identical to within the resolution of the experiment.

In this region the dynamics of the individual oscillators are not changed as the coupling is increased; rather, the coupling simply brings them into synchronization and then into the same phase.

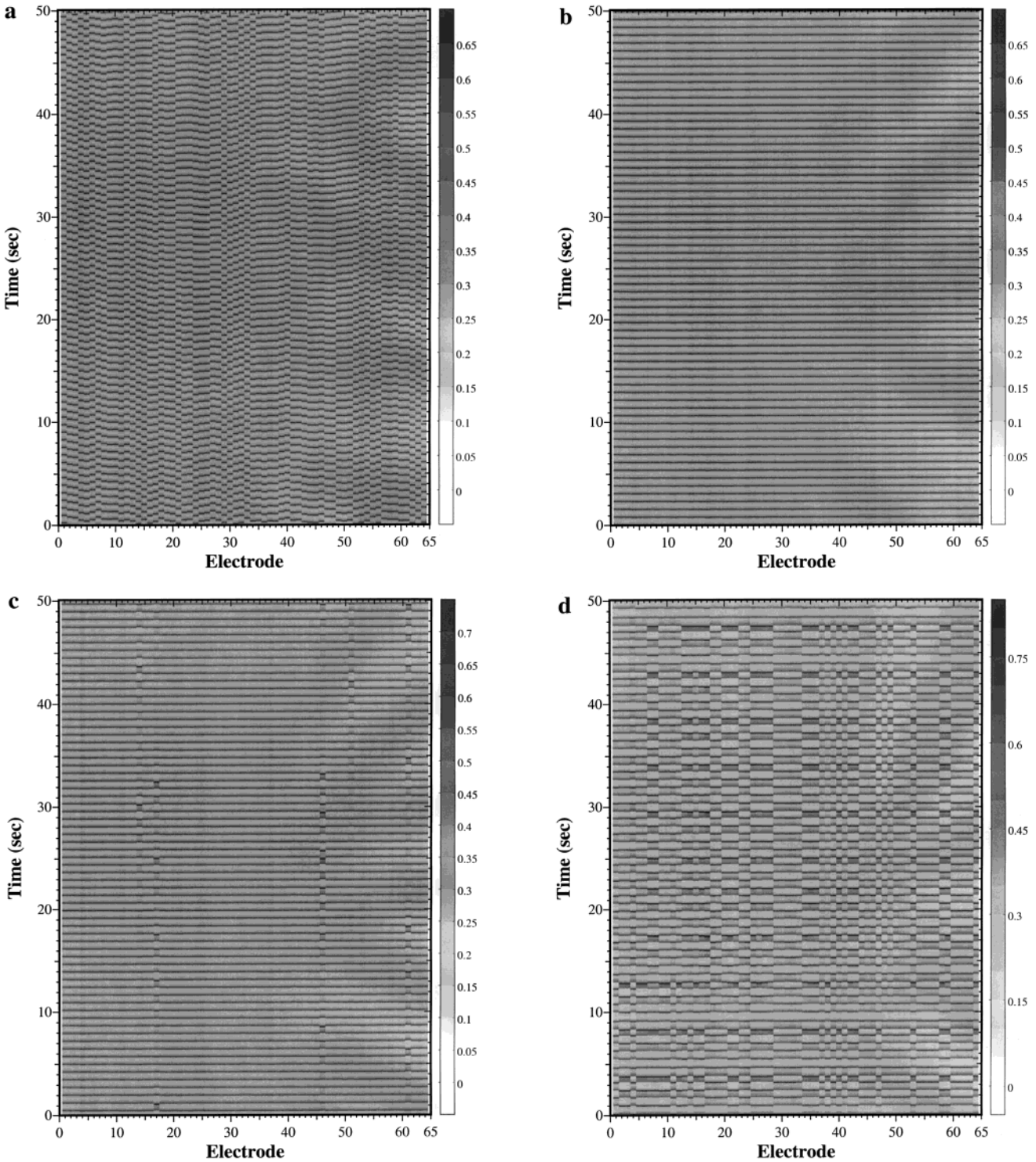

Figure 8. 64-electrode array, relaxation oscillations ($V = 1.43$ V, $R_{eq} = 906$ Ω). Current as function of space/time; dark corresponds to high current. (a) $\epsilon = 0.0$; (b) $\epsilon = 0.28$; (c) $\epsilon = 0.34$; (d) $\epsilon = 0.67$; (e) $\epsilon = 0.78$; (f) $\epsilon = 0.95$; (g) $\epsilon = 1.0$.

Similar experiments have been carried out with the smaller arrays with qualitatively similar results. Some time series for the two-electrode set are presented in Figure 4. When $\epsilon = 0.0$ the individual currents are of course not synchronized (Figure 4a). The amplitude of the oscillation is approximately the same, but their frequencies differ from each other by a few percent (2% at $V = 1.257$ V, $R_{eq} = 260$ Ω). Therefore the total current is quasiperiodic (or periodic with large period). This shows that the inherent local (through diffusion) and long-range (through migration) coupling is very weak. It cannot synchronize even the simple periodic behavior. If ϵ is increased, the oscillations synchronize at a low value of 0.03 (Figure 4b). Above this value the oscillations are synchronized with equal frequencies and amplitudes (Figure 4c). In general, the degree of coupling (the value of epsilon) required to synchronize the oscillators increases with increasing size of the array.

Relaxation Oscillations. Relaxation oscillations occur at potentials cathodic to the saddle-loop bifurcation. We start with some results obtained at potentials very close to the saddle-loop bifurcation.

Results obtained with the two-electrode array are presented in Figure 5. At $\epsilon = 0.0$ (Figure 5a) a quasiperiodic behavior in

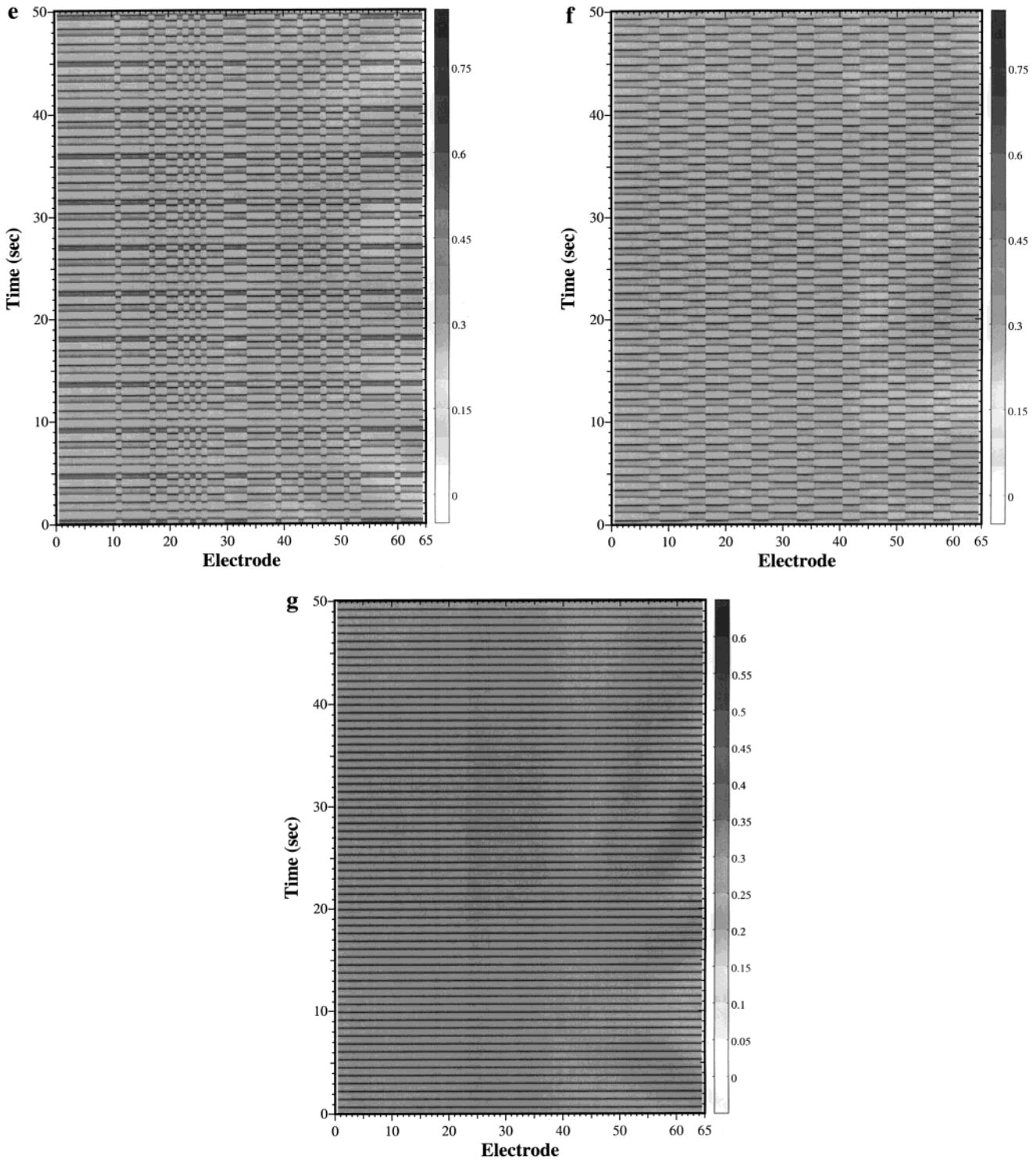

Figure 8 (continued).

total current is observed. At larger coupling ($\epsilon = 0.6$, Figure 5b) antiphase periodic oscillations develop. (We show the behavior for lower coupling strengths below for larger arrays.) The two electrodes alternately go through a maximum in current. The total current, of course, appears to be a simple oscillation although alternate maxima are produced by the two electrodes. With further increase in the coupling, irregular oscillations are developed (Figure 5c). If ϵ is further increased (Figure 5d), periodic total current and periodic local currents are observed again. Note, however, the more complex nature of the individual currents (compared to Figure 5b); in Figure 5d the local currents go through alternating large and small maxima. Even for the strongest coupling at $\epsilon = 1.0$ the two oscillators are not in phase but are rather 180 degrees apart.

The three-electrode array (Figure 6) represents a situation in which some types of symmetric patterns cannot develop since the number of electrodes is odd. As before, at $\epsilon = 0.0$ the electrodes are not synchronized. We show the behavior with added coupling using space−time plots in which the dark shading corresponds to higher current. At $\epsilon = 0.2$ (Figure 6a) the electrodes become synchronized. With increasing ϵ (Figure 6b), a (2,1) cluster formation occurs in which two of the electrodes have identical currents. The clusters break up at higher coupling strengths and irregular oscillations can be observed

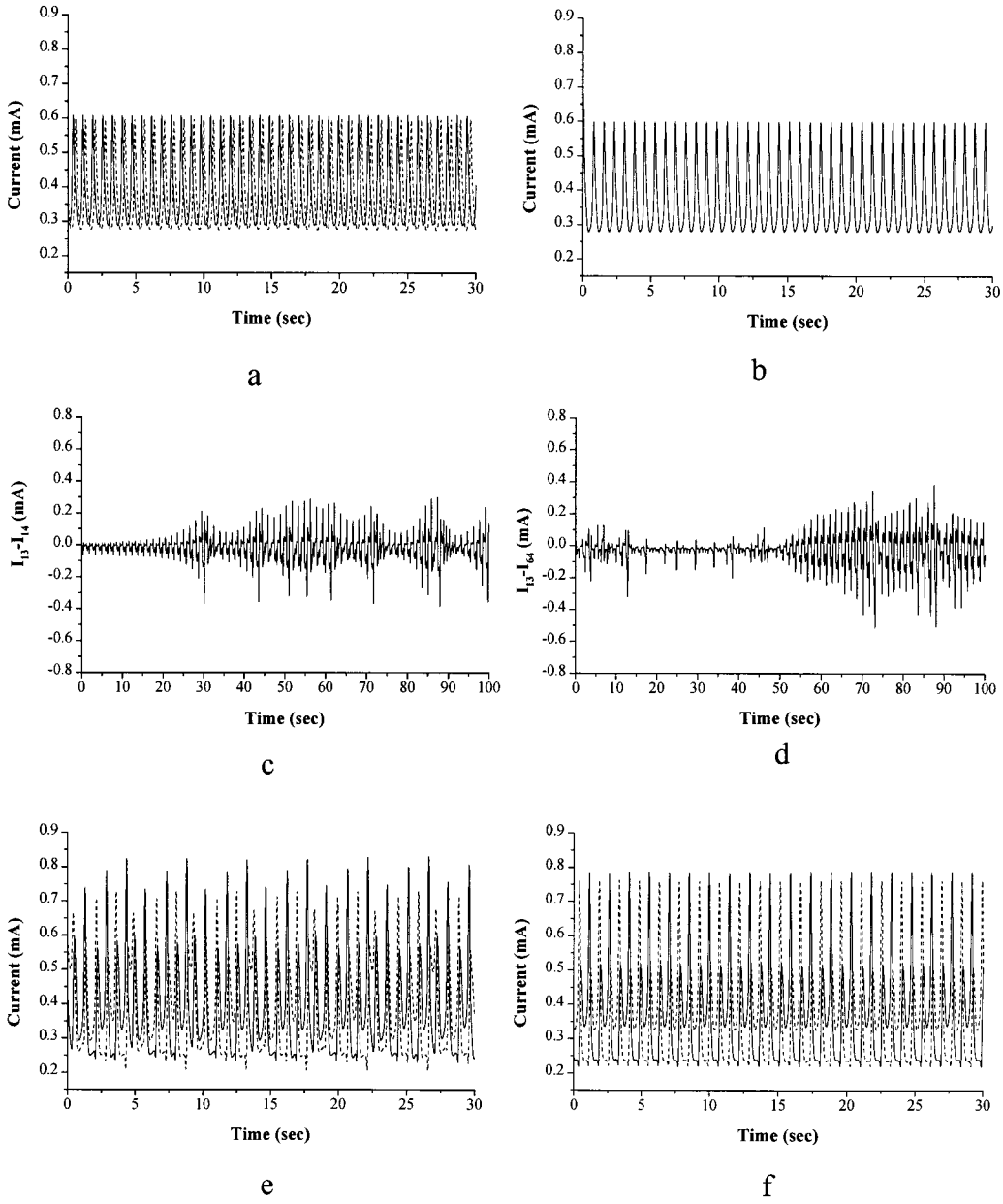

Figure 9. 64-electrode array, relaxation oscillations ($V = 1.43$ V, $R_{eq} = 906\ \Omega$). Currents of individual electrodes corresponding to Figure 8. (a) $\epsilon = 0.0$ (currents of two electrodes); (b) $\epsilon = 0.28$; (c) $\epsilon = 0.34$ (difference between currents of electrodes number 16 and number 61); (d) $\epsilon = 0.67$ (difference between currents of electrodes number 13 and number 64); (e) $\epsilon = 0.78$ (currents of electrodes in each of the two clusters); (f) $\epsilon = 0.95$, (currents of electrodes in each of the two clusters).

for $0.5 < \epsilon \leq 0.85$. At $\epsilon = 0.9$ the clusters (2,1) redevelop. Even at the strongest coupling ($\epsilon = 1.0$, Figure 6d), the clusters remain; the coupling is not strong enough to produce a uniform state.

Symmetric clusters can be observed in the four-electrode setup (Figure 7). For $\epsilon = 0.22$ the oscillations are synchronized as seen in the space−time plot of Figure 7a. As ϵ is increased further (to 0.44) irregular oscillations develop. The irregular oscillations occur over a wide range of the coupling parameter and are shown for $\epsilon = 0.67$ in Figure 7b. The oscillations are irregular, but transient clusters of electrodes with the same currents can be observed. The transient nature of the cluster formation can been seen in Figure 7e in which the difference of currents of two of the electrodes is shown. Note that the behavior of the two electrodes remains fairly close together for a finite time before diverging again. This intermittent behavior continues, that is, the current on two electrodes comes together, remains together for a while, and then diverges. At the strongest coupling, $\epsilon = 1.0$, two clusters (each consisting of two electrodes) appear. Since there are two clusters among the four electrodes, only three possible permutations are possible. Two of these are shown in Figures 7c and 7d. In the former the clusters consist of electrodes (1,3) and (2,4). In the latter the arrangement is (1,4) and (2,3). The dynamics of the two cases are of course identical. In both cases antiphase oscillations are seen.

In the examples shown in Figures 5 through 7 the applied potential was close to the value at which the saddle-loop bifurcation occurs (within 60 mV). Under these conditions complete synchronization to a single uniform state does not occur at maximum external global coupling ($\epsilon = 1.0$). If the applied potential is a little lower, i.e., so that we are farther from the saddle-loop bifurcation, then synchronized periodic oscillations were observed at $\epsilon = 1.0$.

We now turn to coupled relaxation oscillations on the 64-electrode array, first at a potential (1.43 V) somewhat removed

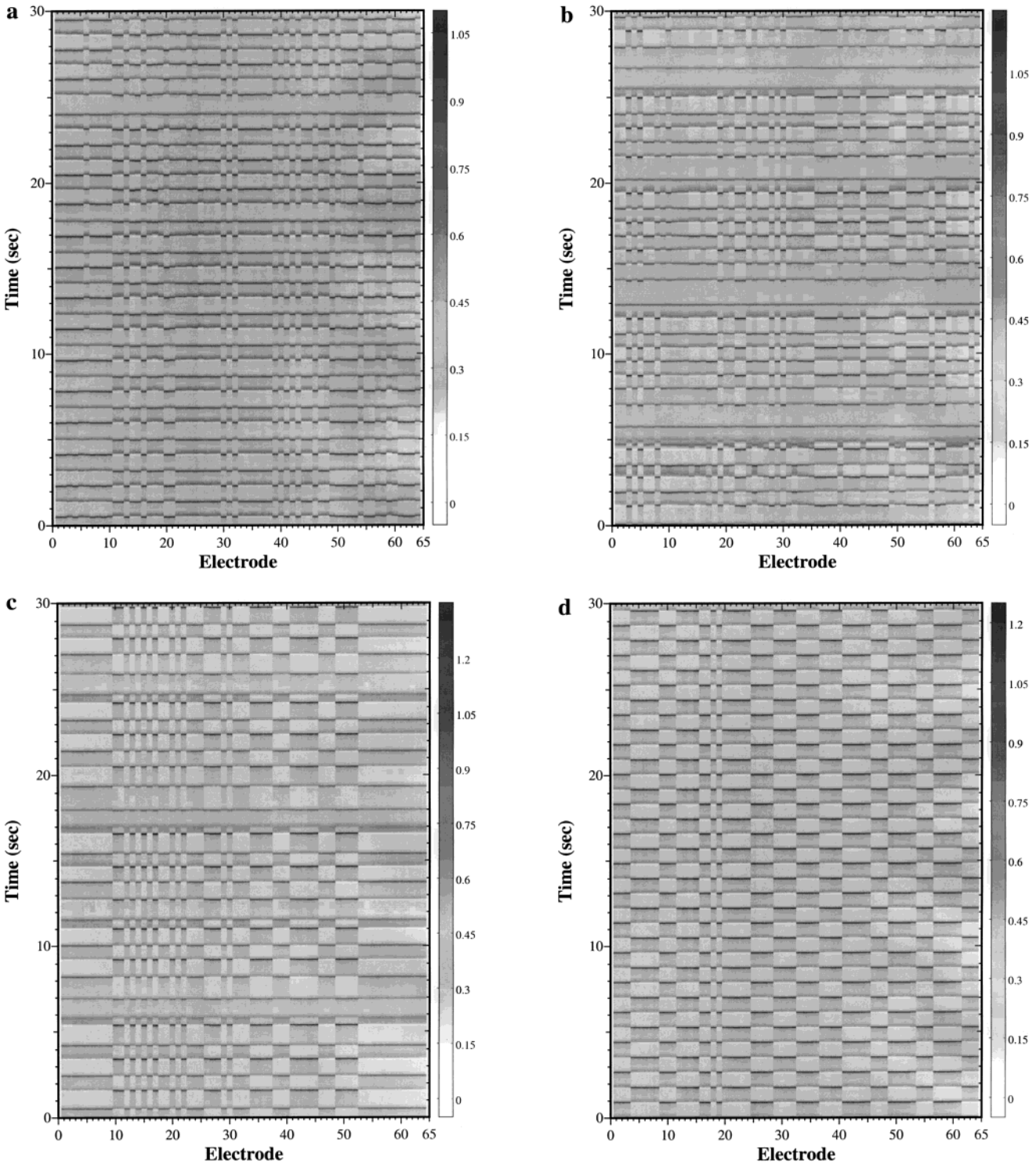

Figure 10. 64-electrode array, relaxation oscillations ($V = 1.53$ V, $R_{eq} = 906\ \Omega$). Current as function of space/time; dark corresponds to high current. (a) $\epsilon = 0.67$; (b) $\epsilon = 0.78$; (c) $\epsilon = 0.89$; (d) $\epsilon = 0.95$.

from the saddle-loop bifurcation and then to one (1.53 V) that is very close.

For no added global coupling ($\epsilon = 0.0$), there is again a distribution in frequency as was the case with the harmonic oscillations. At V = 1.43 V on the 64-electrode array, the mean frequency is 1.32 Hz and the standard deviation is about 0.01 at $\epsilon = 0.0$. Synchronization occurs by $\epsilon = 0.11$ and the phases become identical within experimental resolution by $\epsilon = 0.28$.

The results of a series of experiments with the 64-electrode array at V = 1.43 V with increasing coupling strength are presented in Figures 8 and 9 where currents of many electrodes are seen in space−time plots and the currents of individual electrodes are shown as time series, respectively. The behavior with no added global coupling ($\epsilon = 0.0$) is shown in Figures 8a and 9a. At $\epsilon = 0.28$ (Figures 8b, 9b) the elements are synchronized and the oscillations are similar to the uncoupled individual behavior. As the coupling strength is increased the synchronized behavior begins to break up. The beginning of the breakup can be seen in Figure 8c for $\epsilon = 0.34$. In this case only a small number of the elements move in and out of the dominant synchronized state; the difference between the currents of two electrodes is seen in Figure 9c. This type of behavior

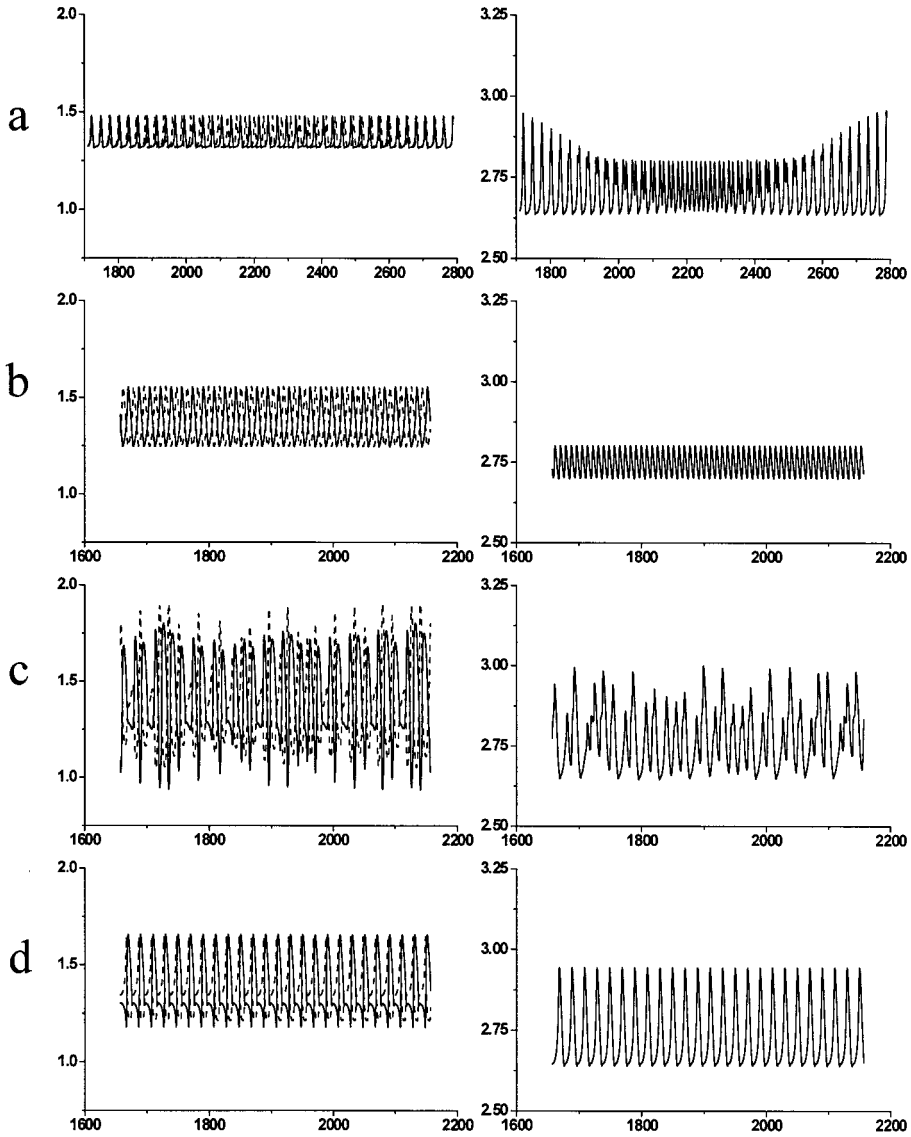

Figure 11. Simulations (current vs time). Two electrodes close to saddle-loop bifurcation ($V = 65.7$, $R_{eq} = 50$). Individual (left column) and total (right column) currents. (a) $\epsilon = 0.0$; (b) $\epsilon = 0.6$; (c) $\epsilon = 0.8$; (d) $\epsilon = 0.9$.

occurs over a large parameter range, and the tendency for elements to move out of the synchronized state increases with increasing coupling strength. In Figures 8d and 9d the behavior is seen for $\epsilon = 0.67$. Further increase in the coupling strength leads to the formation of clusters, an example of which can be seen in Figures 8e and 9e for $\epsilon = 0.78$. In this case the motions of the two clusters are both periodic (period 6) and there are 26 and 38 elements in the two clusters, respectively. (Other configurations are possible.) With further increase in the coupling strength the cluster formation is maintained. The behavior for $\epsilon = 0.95$ is shown in Figures 8f and 9f. In this case the two clusters of 31 and 33 elements undergo antiphase oscillations. Finally, at the strongest coupling strength, $\epsilon = 1.0$, the oscillators become synchronized (Figure 8g) and the oscillations are again the simple form of the single uncoupled state.

We now turn to the results with the 64-electrode array at V = 1.53 V, i.e., closer to the saddle-loop bifurcation. Current as a function of space/time is presented in Figure 10. We show results only at the higher coupling strengths since these differ qualitatively from those seen in Figure 9. At coupling strengths of $\epsilon = 0.67$ and 0.78 (Figures 10a and 10b) irregular oscillations and unstable clusters occur. Such formation and break-up of the clusters occurs throughout the experiment. As the coupling strength is increased further ($\epsilon = 0.89$ Figure 10c) the clusters become stable although the oscillations are irregular. For the conditions of Figure 10c the two stable clusters have 24 and 40 elements, respectively. Obviously the cluster sizes depend on initial conditions. We have also observed cluster configurations of (22,42) and (26,38) under these conditions. Other configurations certainly are possible in the parameter range where the oscillations are irregular, but we have not made an exhaustive study here. We shall carry out a more complete description of cluster formation in the nickel−sulfuric acid system in a subsequent paper dealing with coupling of chaotic oscillators. With further increase in coupling strength to $\epsilon = 0.95$ (Figure 10d) regular antiphase clusters are observed. The most frequently observed cluster configuration is equally sized clusters (32,32), but other configurations have also been seen. In 15 experiments at the same parameter values with arbitrary initial conditions we observed the cluster configuration (32,32) eight times, (31,33) four times, and (30,34), (29,35), and (28,36) once each. Obviously, under conditions where antiphase oscillations tend to form, the condition in which half the electrodes or surface area is in each cluster is favored; nevertheless, configurations with slightly different areas are also stable. We note also that

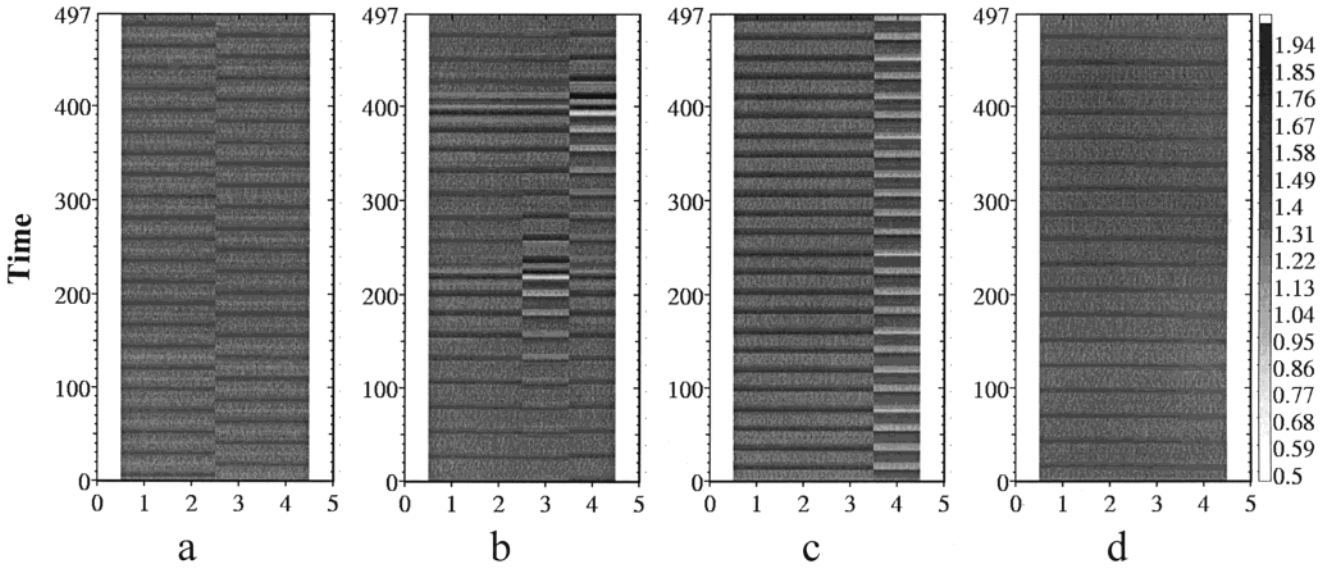

Figure 12. Simulations. Four electrodes close to saddle-loop bifurcation ($V = 65.7$, $R_{eq} = 50$). Current as function of space/time; dark corresponds to high current. (a) $\epsilon = 0.5$; (b) $\epsilon = 0.8$; (c) $\epsilon = 0.85$; (d) $\epsilon = 0.9$.

perturbations of the system can lead to transitions between cluster configurations as is usual in multistable systems; our system is set up so that perturbations can be introduced on one or two of the electrodes in the array, and we have used such perturbations to reach (independently) many of the states listed. Finally, synchronized relaxation oscillations occur at $\epsilon = 1.0$

Model. As a complement to the experimental studies we have carried out some numerical studies of coupled electrochemical oscillators near the saddle-loop bifurcation. For the dynamics of a single element we use the model of anodic electrodissolution of nickel that was proposed by Haim et al.[35] Although the detailed chemistry underlying this model may not be exact,[3] it does reproduce much of the dynamics of a uniform oscillating system describable by a set of ODEs. We apply their model to electrode arrays to capture the main dynamical features of the coupled oscillators. The original dimensionless model is written for three dependent variables: e is the dimensionless potential of the electrode and Ω and η are the surface coverage of different chemical species (NiO+NiOH and NiO, respectively), The model (corresponding to potentiostatic control) is as follows:

$$\frac{de}{dt} = \frac{V - e}{R} - i_F(\Theta,\eta)$$

$$\Gamma_1 \frac{d\Theta}{dt} = \frac{\exp(0.5e)}{1 + C_h \exp(e)}(1 - \Theta) - bC_h\eta \exp(e)$$

$$\Gamma_2 \frac{d\eta}{dt} = \exp(2e)(\Theta - \eta) - cC_h\eta \exp(e) \qquad (4)$$

where V is the dimensionless circuit potential and R is the dimensionless series resistance. The Faradaic current (i_F) is expressed as

$$i_F = \left(\frac{C_h \exp(0.5e)}{1 + C_h \exp(e)} + a \exp(e)\right)(1 - \Theta) \qquad (5)$$

The values $C_h = 1600$, $a = 0.3$, $b = 6 \times 10^{-5}$, $c = 1 \times 10^{-3}$, $\Gamma_1 = 1 \times 10^{-2}$, $\Gamma_2 = 1.00$ are used in the present study.

For an electrode array there are n coupled equations:

$$\frac{de_k}{dt} = \frac{V - e_k}{R_{eq}} + K\sum_{l=1}^{n}(e_l - e_k) - i_{F,k}(\Theta_k,\eta_k) \qquad (6)$$
$$k = 1,...,n$$

where K is a coupling constant. By analyzing the structure of the connected resistors (see Figure 2) K can be related to ϵ for the case where the individual resistors are the same for each electrode:

$$K = \frac{1}{nR_{eq}} \frac{\epsilon}{(1 - \epsilon)} \qquad (7)$$

where ϵ is the coupling coefficient defined in eq 3. If $\epsilon = 0$ then obviously $K = 0$ also; this represents uncoupled oscillators. As $\epsilon \rightarrow 1$, then $K \rightarrow \infty$ representing a situation in which the electrode array acts as one large electrode. In this respect the model overestimates the coupling strength at $\epsilon = 1$ because it neglects the potential drop across the electrolyte. The assumption approximates the conditions of our experiments because the potential drop across the electrolyte is much smaller than that of the resistors. But we should keep in mind that the experimental $\epsilon = 1$ case would relate more closely to a value in the model of slightly under one.

Since the oscillators in the experiments are heterogeneous, we take slightly different parameter values for each of the oscillators in the coupled case. Although several choices might be possible, we simply took different values of Γ_1 and Γ_2 for the different electrodes. This was done in a way so that the average value is the defined nominal values of the parameters. Numerical simulations were carried out for the two- and four-electrode arrays. For the two-electrode array Γ_1 and Γ_2 were 0.25% larger than the mean for one electrode and 0.25% smaller for the other. In case of the four-electrode array the parameters were adjusted by 0.25%, 0.125%, −0.125%, and −0.25%, respectively.

We take a value of $R_{eq} = 50$, in which case the model exhibits a Hopf bifurcation at $V = 17.0$ and a saddle-loop bifurcation at $V = 66.0$. Slightly above the Hopf bifurcation the electrode arrays synchronize at values of ϵ in the range of 0.2 to 0.3. Some results close to the saddle-loop bifurcation are shown in Figure 11 for the two-electrode array. At $\epsilon = 0$ the electrodes are unsynchronized. With increasing ϵ antiphase periodic

oscillations develop (Figure 11b), and with further increasing ϵ irregular oscillations are observed (Figure 11c). At still higher coupling strength (Figure 11d) periodic antiphase oscillations again develop.

Cluster formation was observed in the four-electrode model (Figure 12). With increasing values of the coupling parameter ϵ, one obtains antiphase periodic oscillations, irregular transient clusters, larger amplitude antiphase clusters, and synchronized relaxation oscillations. The last three in the sequence are consistent with the experimental results found near the saddle-loop bifurcation.

Concluding Remarks

Since we are dealing with a real electrochemical system, the reacting surface is somewhat heterogeneous and thus the elements in the array are slightly different. It is impossible to make two equal electrodes: their size and surface structures vary somewhat. In addition, there is a small amount of noise intrinsic to the system. When our global coupling parameter (ϵ) is zero the amount of coupling under the conditions of these experiments is small and the elements oscillate almost independently with frequencies distributed about some mean.

Adding global coupling to the arrays of harmonic oscillators tends to synchronize them. As the coupling is increased from zero the distribution of frequencies becomes narrower until synchronization is attained; further increase brings the phases together. There is no qualitative change in the dynamics of an individual element. Each remains a harmonic oscillator and only the frequency and amplitude are changed somewhat as the coupling is increased. These results are consistent with the theory of coupled oscillators that has been discussed by several investigators.[36,37] The spread of frequencies and the degree of coupling required for synchronization give some measure of the degree of heterogeneity of the system.

When the relaxation oscillators that occur here near the saddle-loop bifurcation are coupled, the situation is somewhat more complicated. The nature of the transitions depends not only on the coupling strength but of course also on other parameters such as applied potential that influence the dynamics. Nevertheless, as the added global coupling strength is increased from zero there is a tendency for the system to synchronize. This synchronized state then breaks up with increasing coupling. Irregular behavior including transient clusters then form; in this region clusters form but are not stable so that the clusters form, disappear, and then form again. At stronger coupling the clusters become stable; these stable clusters can consist of individual currents that are either irregular or periodic with higher period. Multistability occurs in this region, i.e., many cluster configurations are possible. At higher coupling strengths antiphase oscillations occur; in this case the clusters are made up of an equal or approximately equal number of oscillators. Strong coupling synchronizes the oscillators; in this case the individual oscillations are simple and resemble those of the uncoupled base state.

Simulations based on coupled electrochemical oscillators reproduced the main dynamical features: irregular oscillations and cluster formation.

Cluster formation has been studied extensively in simulations of coupled chaotic maps[38] and differential equations.[39] In a recent paper we presented experimental results on synchronization and cluster formation of chaotic electrochemical oscillators.[40]

Acknowledgment. This work was supported by the National Science Foundation and the Fulbright Hungarian−American Exchange Program.

References and Notes

(1) Wojtowicz, J. In *Modern Aspects of Electrochemistry*; Bockris, J. O., Conway, B. E., Eds.; Butterworth: London, 1973; p 4333.
(2) Hudson, J. L.; Tsotsis, T. T. *Chem. Eng. Sci.* **1994**, *49*, 1943.
(3) Koper, M. T. M. *Adv. Chem. Phys.* **1996**, *92*, 161.
(4) Koper, M. T. M. *J. Chem. Soc., Faraday Trans.* **1998**, *94*, 1369.
(5) Krischer, K. In *Modern Aspects of Electrochemistry*; Bockris, J. O.'M., Conway, B. E., White, Eds.; Plenum Press: New York, 1998; Vol 32.
(6) Hudson, J. L. *IMA Volume in Mathematics and its Applications 115*; Golubitsky, M., Luss, D., Strogatz, S. H., Eds.; Springer: Berlin, 1999; p 137.
(7) Flätgen, G.; Krischer, K. *J. Chem. Phys.* **1995**, *103*, 5428.
(8) Flätgen, G.; Krischer, K. *Phys. Rev. E* **1995**, *51*, 3997.
(9) Mazouz, N.; Krischer, K.; Flätgen, G.; Ertl, G. *J. Phys. Chem. B* **1997**, *101*, 2403.
(10) Mazouz, N.; Flätgen, G.; Krischer, K.; Kevrekidis, I. G. *J. Electrochem. Soc.* **1998**, *145*, 2404.
(11) Otterstedt, R. D.; Plath, P. J.; Jaeger, N. I.; Sayer, J. C.; Hudson, J. L. *Chem. Eng. Sci.* **1996**, *51*, 1747.
(12) Chazalviel, J.-N.; Ozanam, F. *J. Electrochem. Soc.* **1992**, *139*, 2501.
(13) Nakabayashi, S.; Baba, R.; Shiomi, Y. *Chem. Phys. Lett.* **1998**, *287*, 632.
(14) Nakabayashi, S.; Zama, K.; Hosaki, K. *J. Electrochem. Soc.* **1996**, *143*, 2258.
(15) Mukouyama, Y.; Hommura, H.; Matsuda, T.; Yae, S.; Nakato, Y. *Chem. Lett.* **1996**, *463*.
(16) Matsuda, T.; Mukouyama, Y.; Hommura, H.; Yae, S.; Nakato, Y. *J. Electrochem. Soc.* **1997**, *144*, 2996.
(17) Grauel, P.; Christoph, J.; Flätgen, G.; Krischer, K. *J. Phys. Chem. B* **1998**, *102*, 10264.
(18) Christoph, J.; Otterstedt, R. D.; Eiswirth, M.; Jaeger, N. I.; Hudson, J. L. *J. Chem. Phys.* **1999**, *110*, 8614.
(19) Mazouz, N.; Flätgen, G.; Krischer, K. *Phys. Rev. E* **1997**, *55*, 2260.
(20) Otterstedt, R. D.; Jaeger, N. I.; Plath, P. J.; Hudson J. L. *Chem. Eng. Sci*. **1999**, *54*, 1221.
(21) Eiswirth, M.; Möller, P.; Wetzl, K.; Imbihl, R.; Ertl, G. *J. Chem.* **1989**, *90*, 510.
(22) Veser, G.; Mertens, F.; Mikhailov, A. S.; Imbihl, R. *Phys. Rev. Lett.* **1993**, *71*, 935.
(23) Mertens, F.; Imbihl, R.; Mikhailov, A. *J. Chem. Phys.* **1994**, *101*, 9903.
(24) Graham, M. D.; Middya, U.; Luss, D. *Phys. Rev. E* **1993**, *48*, 2917.
(25) Liauw, M. A.; Somani, M.; Annamalai, J.; Luss, D. *AIChE Journal* **1997**, *43*, 1519.
(26) Somani, M.; Liauw, M. A.; Luss, D. *Chem. Eng. Sci.* **1997**, *52*, 2331.
(27) Middya, U.; Luss, D. *J. Chem. Phys.* **1994**, *100*, 6386.
(28) Middya, U.; Luss, D.; Sheintuch, M. *J. Chem. Phys.* **1994**, *100*, 3568.
(29) Fei, Z.; Kelly, R. G.; Hudson, J. L. *J. Phys. Chem.* **1996**, *100*, 18986.
(30) Fei, Z.; Hudson, J. L. *Ind. Eng. Chem. Res.* **1998**, *37*, 2172.
(31) Fei, Z.; Green, B. J.; Hudson. J. L. *J. Phys. Chem. B* **1999**, *103*, 2178.
(32) Lev, O.; Wolffberg, A.; Sheintuch, M.; Pismen, L. M. *Chem. Eng. Sci.* **1988**, *43*, 1339.
(33) Lev, O.; Sheintuch, M.; Pismen, L. M.; Yarnittzky, H. *Nature* **1988**, *336*, 458.
(34) Lev, O.; Sheintuch, M.; Yarnittzky, H.; Pismen, L. M. *Chem. Eng. Sci.* **1990**, *45*, 839.
(35) Haim, D.; Lev, O.; Pismen, L. M.; Sheintuch, M. *J. Phys. Chem.* **1992**, *96*, 2676.
(36) Kuramoto, Y. *Chemical Oscillations, Waves and Turbulence*; Springer: Berlin, 1984.
(37) Winfree, Arthur T. *The Geometry of Biological Time*; Springer: New York, 1980.
(38) Kaneko, K. *Physica D* **1989**, *34*, 1.
(39) Zanette, D. H.; Mikhailov, A. S. *Phys. Rev. E* **1998**, *57*, 276.
(40) Wang, Wen; Kiss, István, Z.; Hudson, J. L. *Chaos*, in press.